*Article*

# High-Temperature Diffusion Bonding of Ti–6Al–4V and Super-Duplex Stainless Steel Using a Cu Interlayer Embedded with Alumina Nanoparticles

**Kavian O. Cooke** [1,*] , **Anthony Richardson** [1] , **Tahir I. Khan** [1] **and Muhammad Ali Shar** [1,2]

[1] Faculty of Engineering and Informatics, University of Bradford, Richmond Road, Bradford BD7 1DP, UK; anthony.richardson@cranfield.ac.uk (A.R.); tkhan20@bradford.ac.uk (T.I.K.); M.Baloch@bradford.ac.uk (M.A.S.)

[2] King Abdullah Institute for Nanotechnology, King Saud University, Riyadh 11451, Saudi Arabia

\* Correspondence: k.cooke1@bradford.ac.uk

check for updates

**Abstract:** In this study, Ti–6Al–4V alloy was diffusion bonded to super-duplex stainless steel (SDSS) using an electrodeposited Cu interlayer containing alumina nanoparticles to determine the effects of bonding parameters on the microstructural evolution within the joint region. The results of the study showed that the homogeneity of the joint is affected by the bonding time and bonding temperature. The results also showed that when a $Cu/Al_2O_3$ interlayer is used, Ti–6Al–4V alloy can be successfully diffusion bonded to SDSS at temperatures above 850 °C. The combination of longer bonding time and high bonding temperature leads to the formation of various intermetallic compounds within the interface. However, the presence of the $Al_2O_3$ nanoparticles within the interface causes a change in the volume, size, and shape of the intermetallic compounds formed by pinning grain boundaries and restricting grain growth of the interlayer. The variation of the chemical composition and hardness across the bond interface confirmed a better distribution of hard phases within the joint center when a $Cu/Al_2O_3$ interlayer was used.

**Keywords:** stainless steel; titanium; diffusion bonding; nanoparticles; intermetallic compounds; grain size reduction

## 1. Introduction

Advanced alloys of titanium and stainless steel are widely regarded as high-strength, corrosion-resistant materials that find applications in industries such as biomedical, aerospace, automotive, and oil and gas. The growth in the demand for higher-performing multicomponent structures and mechanical systems necessitates the combination of these advanced alloys into superstructures containing multiple materials of uniquely differing chemical, thermal, and thermomechanical properties [1,2]. Currently, structures made with materials of similar types are joined using traditional welding technologies such as arc welding [3], laser welding [4], spark plasma welding [5], ultrasonic welding [6], etc. The welding of multiple components of structures is still an area that requires extensive research to identify technologies that are capable of welding dissimilar materials without adverse effects given the differences in the properties of the materials [7]. Techniques such as friction stir welding (FSW) [8], friction stir spot welding (FSSW) [9], and ultrasonic welding (USW) [10] have shown potential for producing multicomponent structures; however, there still exist numerous limitations that constrain the successful application of these technologies in industry.

Diffusion bonding is another technique that has demonstrated promise for combining dissimilar metals into hybrid structures while constraining the volume of intermetallic compounds that form at the joint interface [11,12]. There are two variants of the diffusion bonding process: The first is transient

liquid phase bonding, during which liquid may form due to the direct melting of the interlayer or due to eutectic reaction between the interlayer and the base metal [13]. The second variant is solid-state diffusion bonding, in which bonding occurs below the melting points of the base metals or interlayer. Unfortunately, the persistent formation of a continuous layer of intermetallic compounds at the joint interface limits the potential applications of solid-state diffusion bonding.

Recent studies on the transient liquid phase diffusion (TLP) bonding of dissimilar alloys [11,14] have shown that the addition of nanoparticles to the interlayer has the capacity to constrain the size of the intermetallic compounds that form at the interface while disrupting the shape of the intermetallic layer. In these studies, the results show that when nanoparticles were added to the interlayer, the intermetallic compounds that formed at the interface were shorter and more disperse within the joint region [11]. However, the studies were all conducted on relatively low-melting-point nonferrous alloys.

This study investigated the diffusion bonding of Ti–6Al–4V and SDSS using an electrodeposited Cu coating containing 40 nm $Al_2O_3$ particles as a method of disrupting the volume, shape, and size of the intermetallic layers that form at the interface during bonding. The results of this study are significant since it provides a method of controlling or modifying the type and form of intermetallic compounds that form during diffusion bonding of dissimilar alloys.

## 2. Experimental Procedure

### 2.1. Materials

Table 1 shows the composition of the materials studied. Prior to bonding, the Ti–6Al–4V sample was coated with an electrodeposited copper coating (Cu) containing $\alpha$-$Al_2O_3$ nanoparticles having an average diameter of 40 nm. The electrodeposition process was carried out as described in a previously published article [11]. A scanning electron microscopy (SEM) micrograph and energy-dispersive spectroscope (EDS) spectrum of the interlayer confirmed the uniform distribution of nanoparticles within the coating (see Figure 1). The bonds produced using a 5 μm thick $Cu/Al_2O_3$ interlayer were compared to bonds formed using 25 μm thick Cu foil to assess the role of the particles in the bonding process and the properties of the joint interface.

**Table 1.** Chemical composition (wt %) of the alloys studied.

| Alloys | Al | Mn | V | Cr | Ag | Cu | Si | Ni | Mg | Ti | Fe | C | Mo |
|--------|-----|------|---|----|------|------|------|----|-----|------|------|------|----|
| SDSS | 1.1 | 0 | 0 | 25 | 0 | 0.43 | 0.02 | 7 | 0 | 0 | Bal. | 0.03 | 4 |
| Ti–6Al–4V | 6 | 0.23 | 4 | 0 | 0.86 | 0 | 0.15 | 0 | 2.7 | Bal. | 0 | 0 | 0 |
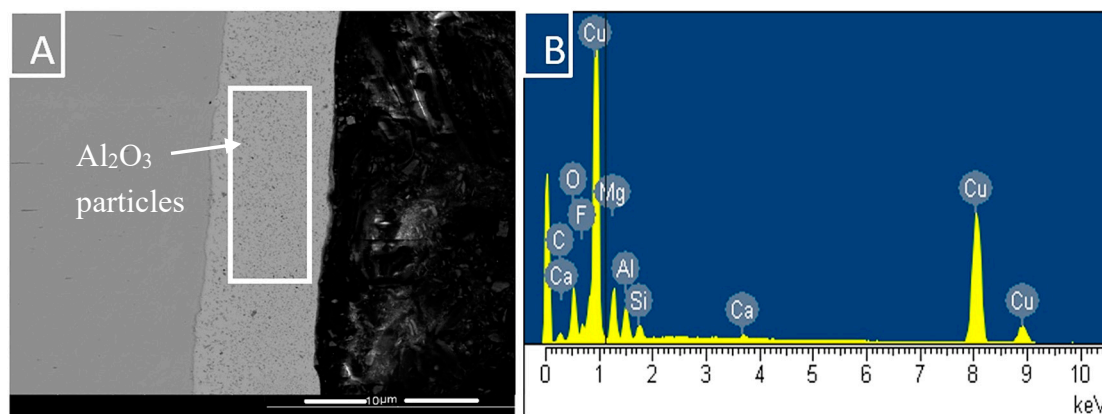


**Figure 1.** (**A**) $Cu/Al_2O_3$ coating deposited on the titanium; (**B**) EDS spectrum of the highlighted region confirming the elements present in the $Cu/Al_2O_3$ coating.

## 2.2. Sample Preparation and Bonding Process

Samples of 10 mm diameter and 7 mm length were prepared from bars of Ti–6Al–4V and duplex stainless steel. The Ti sample was coated for 10 min to deposit the $Cu/Al_2O_3$ coating. A schematic of the process is presented in Figure 2. The coating process was published in a previous article [11]. A hole of 1.5 mm diameter by 3 mm deep was drilled into the Ti sample to accommodate a K-type thermocouple. The faying surfaces were prepared by grinding progressively from 320 to 2500 grit size SiC, polished to 1 μm grit size using particle-impregnated carrier paste, and then cleaned in an acetone bath.
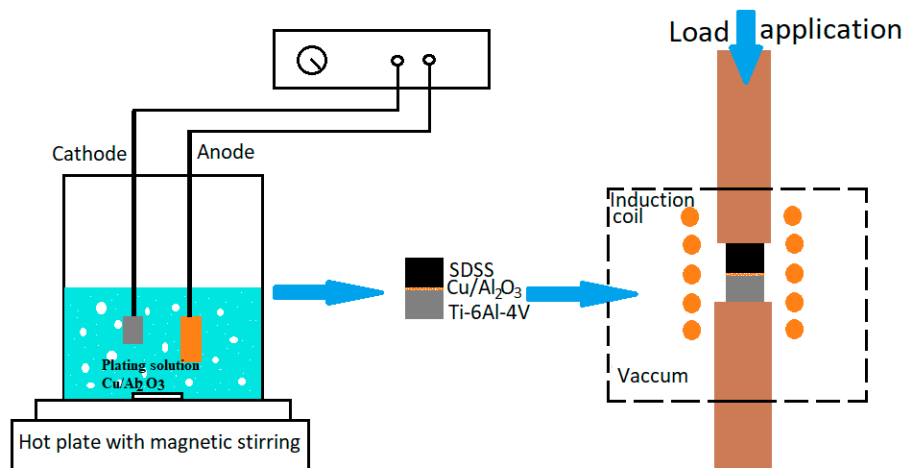


**Figure 2.** Schematic of the coating deposition and bonding process.

Prior to bonding, the samples were assembled at room temperature and then placed on the lower platen within the induction coil, and an ungrounded K-type thermocouple was inserted into the hole located approximately 1 mm from the bonding surface. Once a vacuum of $2 \times 10^{-3}$ Torr was achieved, the assembly was heated to the bonding temperature of 800 °C, 850 °C, or 900 °C. The samples were loaded with 5 MPa and heated to the bonding temperature at a rate of 65 °C/min, then held at that temperature for bonding time of 15, 30, 45, or 60 min. Samples that were diffusion bonded for 15 min or less failed during preparation. Following the diffusion bonding process, the samples were cooled under vacuum to room temperature. Each bonded sample was sectioned transversely to the bond-line by an abrasive saw, following which each haft was mounted in Bakelite. Three samples were prepared for each condition studied. The mounted specimens were prepared by grinding progressively on silicon carbide papers to 2500 grit, followed by a final polish to 1 μm finish.

Hardness testing of the cross section of the joints was performed using a Leitz microhardness tester. Indentations were made at 100 μm spacing using a diamond tip indenter to which a 0.1 kg load was applied for 30 s, after which the length of the diagonals was measured, and the hardness number calculated. Microscopic examination of the bonded joints was performed using a Leitz optical microscope and a scanning electron microscope (SEM) (FEI Quanta 400, Oxfordshire, UK) equipped with an INCA X-sight X-ray. Quantitative compositional analyses were carried out using energy-dispersive spectroscopy (EDS) and a Bruker X-Ray diffractometer (XRD) from 2θ ranging from 10° to 80° and measuring time 1 s per step.

## 3. Results and Discussion

### 3.1. Effect of Bonding Time on the Bond Interface

The influence of bonding time on the microstructure formed within the joint region during diffusion bonding was assessed by varying the bonding time from 15 min to 60 min. Figure 3A shows the SEM micrograph of a sample bonded at 850 °C for 30 min. The joint appears to represent

a homogenous bond between the Ti–6Al–4V alloy and SDSS. However, a thick reaction layer was observed at the interface on the Ti side of the bond. $Al_2O_3$ particles appear to have formed clusters and segregated to the grain boundary regions within the Ti side of the bond. The highlighted region presented in Figure 3A shows an additional reaction layer at the SDSS interface. When the bonding time was increased to 45 min, the width of the interface also increased with the formation of two additional phases within the reaction layer containing dispersed $Al_2O_3$ particles. Microcracking was also observed in this layer of the interface. The fracture may have occurred during the cutting of the sample; these crack patterns, however, suggest that the reaction layer may be brittle. Further increase of the bonding time to 60 min resulted in the formation of four distinct reaction regions at the interface, primarily on the Ti side. While interdiffusion led to the formation of a wide region, labelled A, the nanoparticles appear to have segregated to form a thick layer at the SDSS interface. EDS analysis of the dark grey particles showed that the $Al_2O_3$ particles reacted with Cu and Fe [15,16].
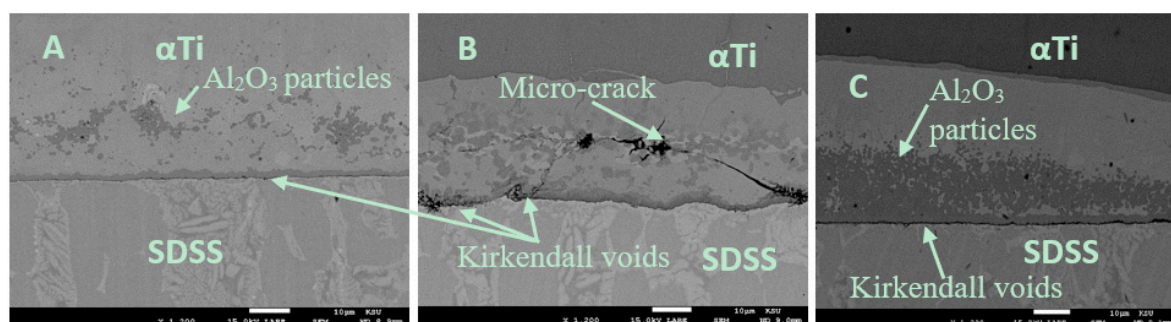


**Figure 3.** Effect of bonding time on the joint zone during diffusion bonding of Ti–6Al–4V and SDSS using a $Cu/Al_2O_3$ interlayer. Each sample was bonded at 850 °C for (**A**) 30 min, (**B**) 45 min, or (**C**) 60 min.

With increasing bonding time, Kirkendall effects were observed to play an important role in the homogeneity of the interfaces. As identified in Figure 3, the formation of voids occurred at the $Cu/Al_2O_3$/SDSS interface, and the volume of voids present in this area increased as the bonding time increased. The formation of these voids was attributed to the interdiffusion of Cu and Fe near the bottom of the $TiCu_2$ layer. The presence of the voids formed at the SDSS interface was attributed to the differences in the rate of diffusion between Cu in Fe and Fe in Cu. Continued interdiffusion during the diffusion bonding process is believed to result in an accumulation of voids at the SDSS interface and blocks the diffusion of Fe, causing the growth of the $TiCu_2$ layer.

*3.2. Effect of Bonding Temperature on the Interface*

The effect of bonding temperature on the microstructural evolution within the joint region was evaluated at bonding temperatures of 800 °C, 850 °C, and 900 °C for 30 min bonding time. Samples bonded at temperatures below 800 °C failed during preparation for testing. For a bonding temperature of 800 °C, three distinct reaction layers were observed at the interface as shown in Figure 4A. These regions were identified by the differences in the shades of the layers formed. The micrograph also shows evidence of incomplete bonding at the SDSS/$Cu/Al_2O_3$ interface due to the presence of several cavities/voids. On the other hand, the Ti/$Cu/Al_2O_3$ interface showed evidence of uniform bonding between the $Cu/Al_2O_3$ interlayer and the Ti base metal. This dissimilarity may be attributed to the differences in the diffusion coefficient of Cu in Fe and Cu in Ti. The literature shows that within the temperature range studied, the diffusivity of Cu in Ti shows fast impurity diffusion when compared to other metals [17]. Further increase of the bonding temperature to 850 °C led to the formation of a uniform bond at both the SDSS/$Cu/Al_2O_3$ and Ti/$Cu/Al_2O_3$ interfaces, as shown in Figure 4B. The $Al_2O_3$ nanoparticles appear to be distributed along the grain boundaries on the Ti side of the bond. When the bonding temperature was further increased to 900 °C, the width of the reaction zones at the Ti/interlayer interface increased in thickness, and a third reaction layer was observed at the

SDSS/interlayer interface (see Figure 4C). According to the Ti–Cu phase diagram, bonding within the temperature range of 870–900 °C would allow for the formation of a eutectic liquid of the form $L = TiCu_4 + Ti Cu_2$. Evidence of the formation of the eutectic liquid is shown in Figure 5A. Additionally, at higher bonding temperatures the $\alpha - \beta$ Ti microstructure forms at the Ti/Cu/Al$_2$O$_3$ interface (see Figure 5B).
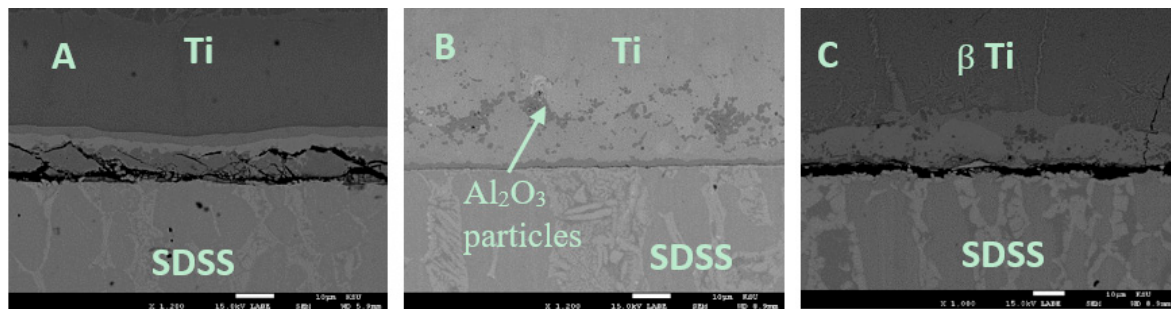


**Figure 4.** SEM micrograph of Ti–6Al–4V and super-duplex stainless steel diffusion bonded for 30 min using a Cu/Al$_2$O$_3$ interlayer at the following temperatures: (**A**) 800 °C, (**B**) 850 °C, (**C**) 900 °C.
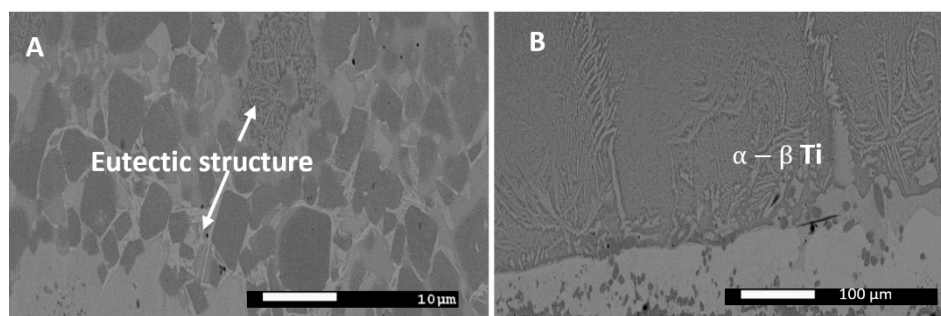


**Figure 5.** SEM micrographs of (**A**) the eutectic structure form at the interface for samples bonded at 900 °C; (**B**) Microstructure on the Ti side of the interface.

### 3.3. Effect of Interlayer Composition on the Bond Interface

The influence of the interlayer composition on the microstructure of the joint region was investigated by comparing bonds formed using an electrodeposited Cu coating containing $\alpha$-Al$_2$O$_3$ nanoparticles (Figure 6A,B) and a 25 µm Cu foil was used as the interlayer (Figure 6C,D). Figure 6A shows the presence of six separate distinct layers, where each layer is distinguishable by the shade of the specific region. These areas were labelled P$_2$–P$_7$. The elemental composition of each phase was identified using EDS and is presented in Table 2. The EDS analysis shows that the composition of P$_1$ is that of the super-duplex stainless steel because of the high Fe and Cr content and low Cu concentration.

The dark grey region P$_2$ is a Cu-rich phase of TiCu$_2$ which contains 67 wt % Cu and 28 wt % Ti. P$_3$ also appears to be a Cu-rich phase with a composition of 33 wt % Ti and 58 wt % Cu and is possibly the same TiCu$_2$ (see Figure 6B). Similar changes were observed for region P$_4$, which had a composition of 41 wt % Ti and 55 wt % Cu, while P$_5$ similarly showed a marginal change in the Ti content. The EDS analysis suggests that both P$_4$ and P$_5$ are TiCu compounds (see Figure 6A). The Ti-rich phase P$_6$ was identified as Ti$_2$Cu into which Cu had diffused. The general trend showed that the Ti content within the reaction layers increased progressively from the steel side of the bond towards the Ti base metal. The region labelled P$_7$ contained spherical particles distributed within the grain boundary region. EDS analysis showed the presence of Al$_2$O$_3$ particles as well as Cu, Ti, and Fe.
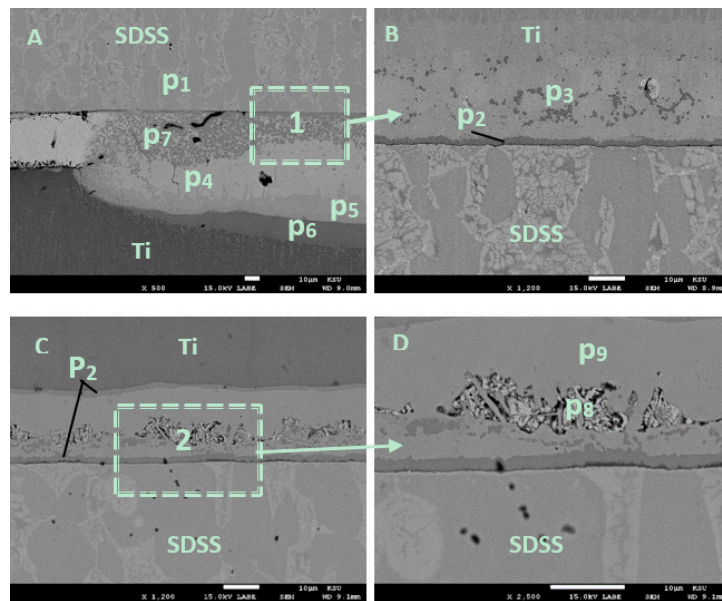
**Figure 6.** Effect of interlayer composition on joint microstructure during diffusion bonding of Ti–6Al–4V and super-duplex stainless steel. The sample was bonded at 850 °C for 30 min. (**A**) Sample bonded using a Cu/Al$_2$O$_3$ coating electrodeposited onto Ti–6Al–4V; (**B**) Detail of Region 1; (**C**) Sample bonded using 25 μm Cu foil; (**D**) Detail of Region 2.

**Table 2.** EDS assessment of the composition of the joint interface (wt %).

| Phase | Al | Ti | V | Fe | Cu | C | Cr | Ni | Possible Phase |
|-------|------|-------|------|-------|-------|------|-------|------|----------------|
| P$_1$ | - | 0.22 | - | 61.57 | 0.68 | 3.51 | 24.45 | 5.73 | |
| P$_2$ | 1.86 | 28.64 | 1.03 | 0.54 | 67.34 | - | - | 0.59 | TiCu$_2$ |
| P$_3$ | 2.43 | 33.78 | 1.24 | 1.26 | 58.45 | 2.34 | - | - | TiCu$_2$ |
| P$_4$ | 0.32 | 41.31 | 0.73 | - | 55.54 | 2.1 | - | - | TiCu |
| P$_5$ | 1.36 | 41.55 | 1.40 | 1.13 | 51.32 | 2.89 | | | TiCu |
| P$_6$ | 5.53 | 79.00 | 4.83 | 0.45 | 10.18 | - | - | - | Ti$_2$Cu |
| P$_7$ | 7.49 | 47.08 | | 1.95 | 40.47 | 1.47 | 1.08 | 0.46 | TiCu/Al$_2$O$_3$ |
| P$_8$ | 1.35 | 41.55 | 1.40 | 1.13 | 51.32 | 2.89 | 0.36 | - | Ti$_x$ Cu$_x$-Fe$_x$ |
| P$_9$ | 2.19 | 54.19 | 1.91 | 0.81 | 37.77 | 2.58 | 0.29 | 0.26 | Ti$_2$Cu |

The Ti/SDSS joint bonded using 25 μm Cu foil presented in Figure 6C shows the presence of five distinct reaction regions identified by the differences in shade, similar to those identified when the Cu/Al$_2$O$_3$ interface was used. EDS analysis of the region labelled P$_8$ suggests that this phase is a ternary compound of the form Ti$_x$Cu$_x$-Fe$_x$. The region labelled P$_9$ is believed to be compound TiCu given the high Ti content recorded (see Figure 6D). A summary of the phases identified is listed in Table 2. The low 0.54–1.95 wt % of Fe recorded within the reaction layer confirms that phases P$_3$, P$_4$, P$_5$, and P$_7$ are likely binary compounds formed from reactions between Ti and Cu. EDS maps of the bond formed using Cu foil as the interlayer showed that the distribution of the elements Fe, Cu, and Ti within the reaction layer (Figure 7) led to the formation of the ternary intermetallic compound labelled at P$_8$: (Ti$_{33}$Cu$_{67}$ − $x$Fe$x$; $1 < x < 2.5$), T$_2$ (Ti$_{40}$Cu$_{60}$ − $x$Fe$x$; $5 < x < 17$), T3 (Ti$_{43}$Cu$_{57}$ − $x$Fe$x$; $21 < x < 24$), τ (Ti$_{37}$Cu$_{63}$ − $x$Fe$x$; $6 < x < 7$), and τ$_1$ (Ti$_{45}$Cu$_{55}$ − $x$Fe$x$; $4 < x < 5$) [18].
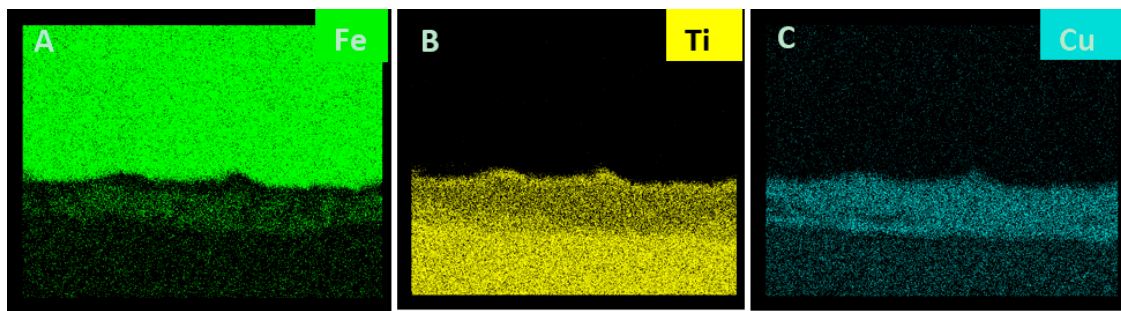
**Figure 7.** EDS maps of Ti–6Al–4V and SDSS joint bonded at 850 °C for 45 min with 25 μm Cu foil. EDS mapping of elements (**A**) iron, (**B**) Titanium, and (**C**) Copper.

EDS line scans presented in Figures 8 and 9 show a visual representation of the variation of the composition across the joint zone and confirm the high concentration of Ti and Cu within the reaction layers. The Ti–Cu phase diagram shown in Figure 10A suggests that within the range of composition listed in Table 2, the compound $TiCu_2$ would form with Cu content varying between 33 wt % and 48 wt %. The compound labelled $P_8$ was only found at the interface when Cu foil was used as the interlayer. This phase has a higher concentration of Fe and is believed to be a ternary intermetallic phase.
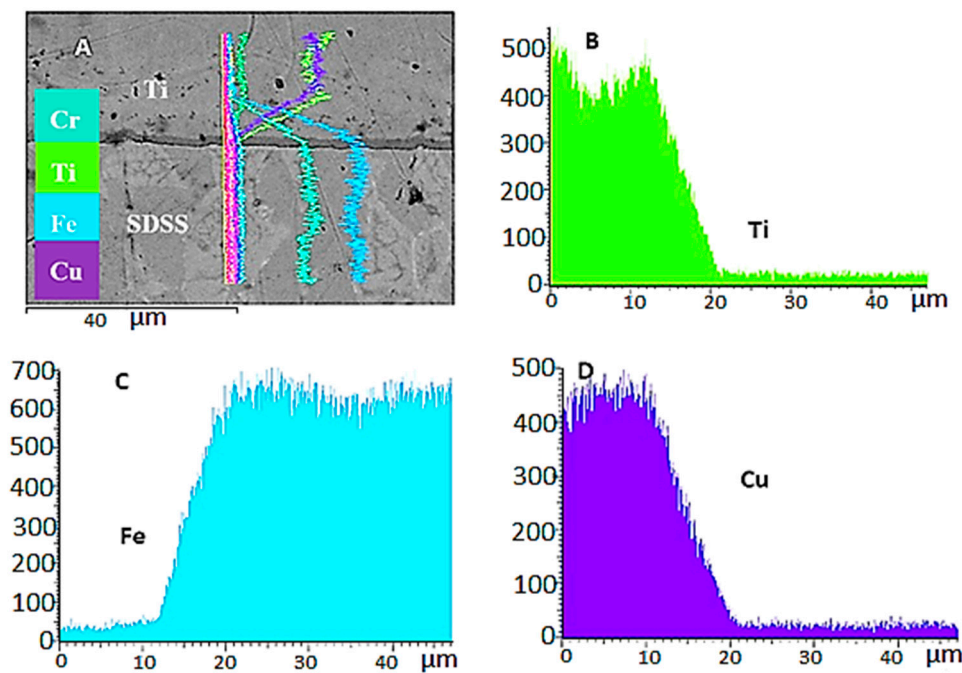


**Figure 8.** (**A**) SEM micrograph of a region on the Ti–6Al–4V and SDSS joint bonded at 850 °C for 45 min with $Cu/Al_2O_3$ coating. EDS line scanning analysis of elements (**B**) Ti, (**C**) Fe, and (**D**) Cu.

These phases are believed to have formed due to the dissolution of approximately 38 wt % of Cu in the cubic Ti–Fe lattice. The Ti–Cu–Fe ternary phase diagram presented in Figure 10B confirms the likelihood of the formation of intermetallic compounds within the temperature range of 800–900 °C [19].

The shape of the compound formed at the interface when the Cu foil was used as the interlayer appears to be a continuous series of brittle plates, which are stacked as shown in Figure 6D. When compared to the bond formed using the $Cu/Al_2O_3$ coating as the interlayer, the nanoparticles are seen to occupy positions around grain boundaries as shown in Figure 6C.
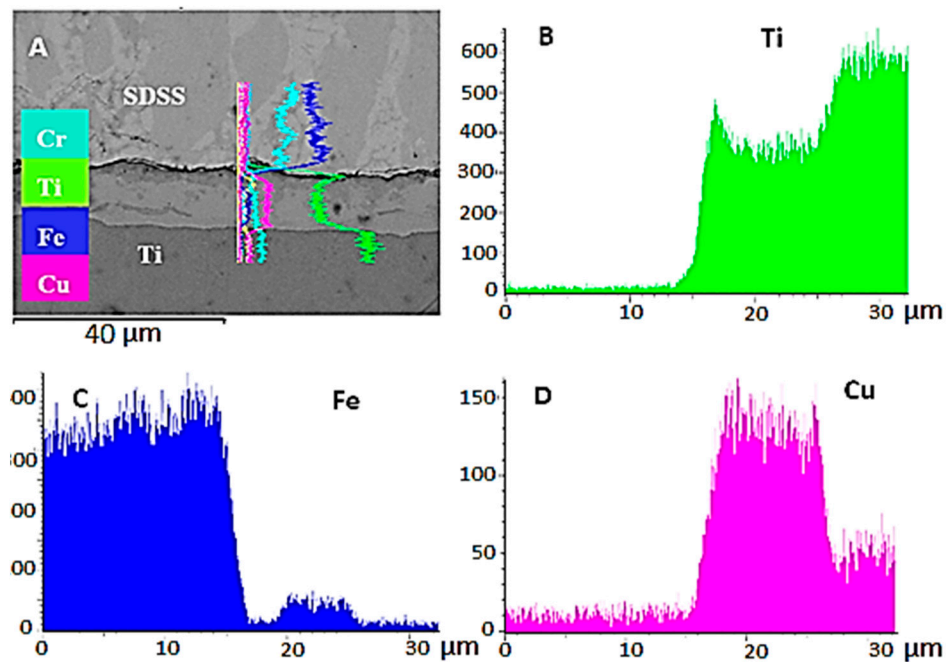
**Figure 9.** (**A**) BSE micrograph of a region on the Ti–6Al–4V and SDSS joint bonded at 850 °C for 45 min with 25 μm Cu foil. EDS line scanning analysis of elements (**B**) Ti, (**C**) Fe, and (**D**) Cu.
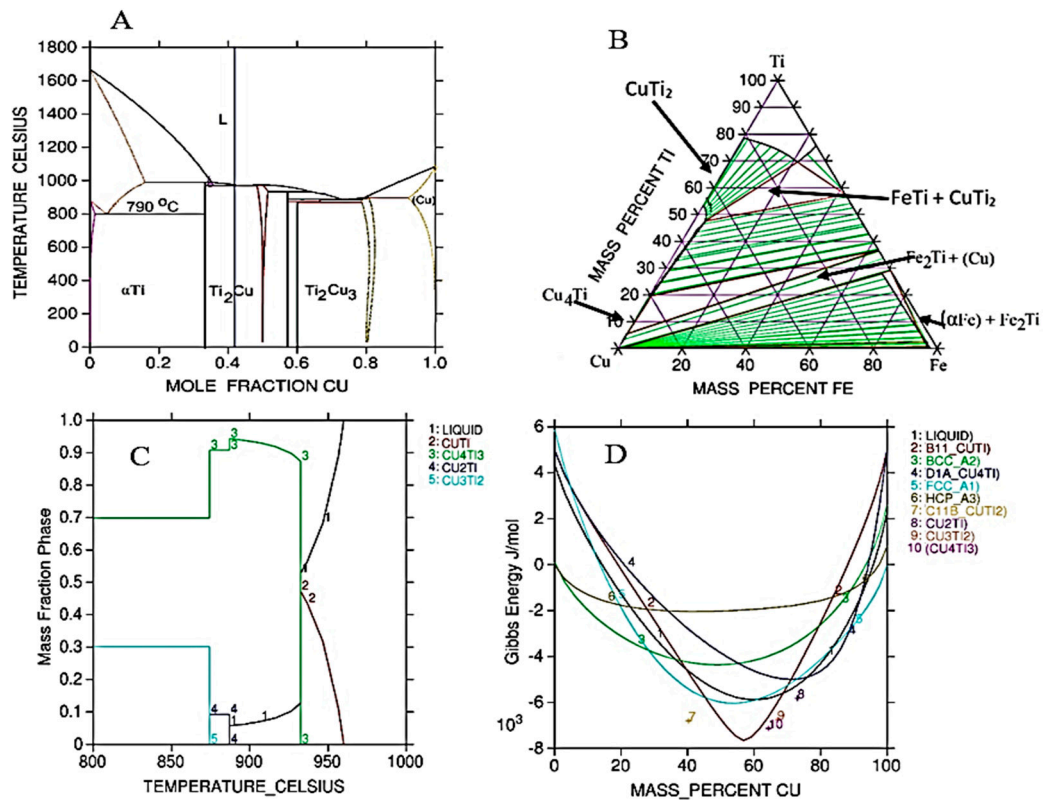


**Figure 10.** (**A**) Ti–Cu binary phase diagram highlighting the composition of the reaction layer formed during the bonding process; (**B**) Cu–Fe–Ti isothermal section at 850 °C; (**C**) Phase fraction as a function of temperature; (**D**) Gibbs free energy curve with respect to the concentration of Cu at a bonding temperature of 850 °C.

The EDS line scans presented in Figure 9 show that a large portion of the reaction layer formed on the Ti side of the bond was promoted by the diffusion of Cu into the Ti base metal, given that Cu diffuses faster into Ti than it does into SDSS. Similar findings were observed when the $Cu/Al_2O_3$ interlayer was used (see Figure 9). The reaction layer was found to have a higher percentage of Cr and Fe, which may suggest that Fe and Cr diffused faster into the $Cu/Al_2O_3$ coating than into the Cu foil.

When the process was modelled using Thermo-Cal, the results showed that within the bonding temperature range studied (850–900 °C) four binary phases are possible; Cu3Ti2, $Cu_2Ti$, $Ti_2Cu$, and $Cu_4Ti_3$, as shown in Figure 10A, support the EDS data. Similar observations were reported by Pardal et al. [3] who studied dissimilar metal joining of Ti and duplex stainless steel using Cu as a transition metal interlayer. A plot of the Gibbs free energy profile shown in Figure 10C,D indicates that several stable phases are likely to form in the Ti–Cu binary system for the bonding temperature range studied. The sequence of phase formation goes from $CuTi_2$ to $Cu_4Ti_3$, $Cu_3Ti_2$, and $Cu_2Ti$. The growth of these phases is believed to be promoted by interdiffusion between Cu and Ti into the reaction layer. The XRD spectrum presented in Figure 11 confirms the presence of $Cu_2Ti$ within the bonded region.
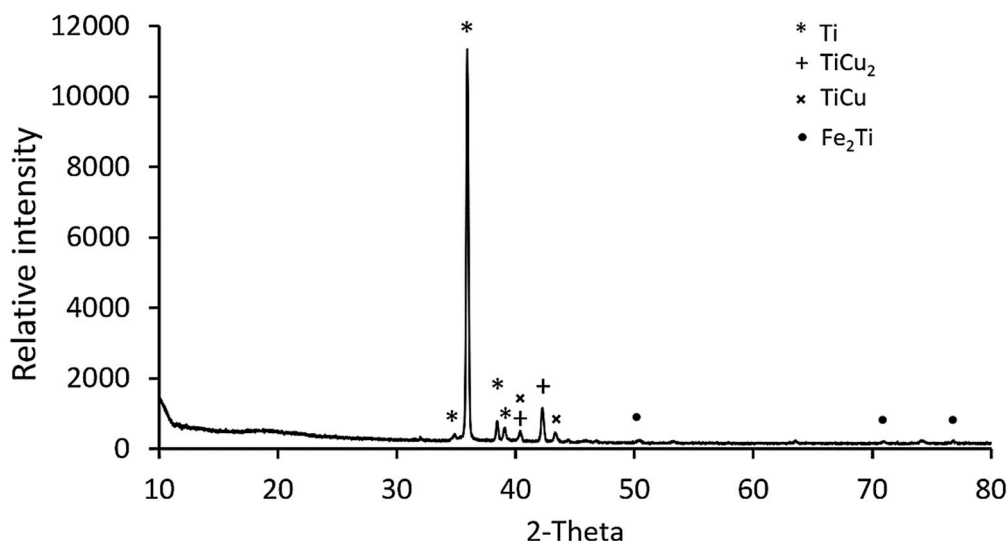


**Figure 11.** XRD spectrum of the Ti–6Al–4V and SDSS joint bonded at 850 °C for 45 min with $Cu/Al_2O_3$ coating.

*3.4. Hardness*

The influence of bonding temperature on variation of the hardness across the bonding interface was evaluated and is presented in Figure 12. The hardness values were measured across the joint starting at 300 μm from the joint center. The results show that the hardness of the Ti base metal fluctuated between 320 and 420 VHN up to 100 μm from the joint center as the bonding temperature was increased from 800 to 900 °C. The hardness within the joint center was also observed to decrease from 634 to 405 VHN when the bonding temperature was increased from 800 to 900 °C. The hardness of the SDSS base metal was found to be higher than that of the Ti base metal, with a hardness value of 387 VHN. The result of the hardness test shows (see Figure 12A) that the hardness within the joint center decreased with increasing bonding temperature. These findings were attributed to increased diffusion rates at higher bonding temperatures leading to homogenization of the bond region.

The effect of bonding time on variation of the hardness across the joint interface was also studied (see Figure 12B). Similarly, the hardness was measured across the joint starting at 300 μm from the joint center as a function of bonding time. The hardness within the joint center increased from 554 to 752 VHN when the bonding time was increased from 30 min of bonding time to 60 min. The maximum hardness of 750 VHN was recorded at the center of the joints bonded for 60 min. The hardness at the center of the bond is believed to have been caused by the formation of the reaction layer made up

of binary and ternary intermetallic compounds as well as $Al_2O_3$ nanoparticles dispersed at the joint interface [20].
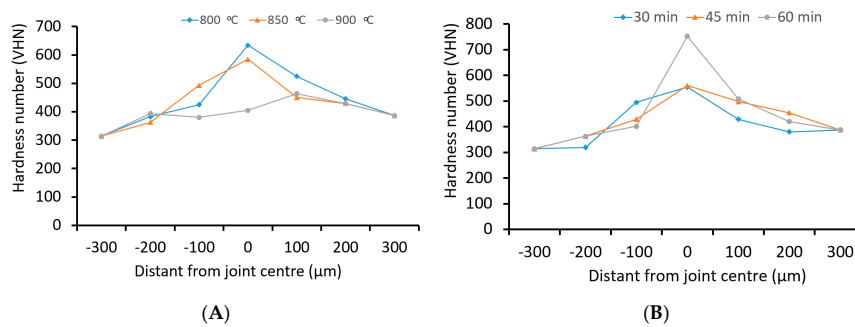


**Figure 12.** (**A**) Hardness measurements for the sample bonded for 30 min as a function of bonding temperature; (**B**) Hardness measurements for the sample bonded at 850 °C as a function of bonding time.

Finally, the impact of interlayer composition on variation of the hardness measurements (see Figure 13) across the joint region was evaluated by comparing the bonds made with $Cu/Al_2O_3$ and Cu foil interlayers. The results show that when the $Cu/Al_2O_3$ interlayer was used, higher hardness values were recorded in the joint region when compared to samples bonded using Cu foil. The results show that the hardness within the joint center was marginally higher when $Cu/Al_2O_3$ coating was used as the interlayer due to the dispersion of hard nanoparticles at the interface.
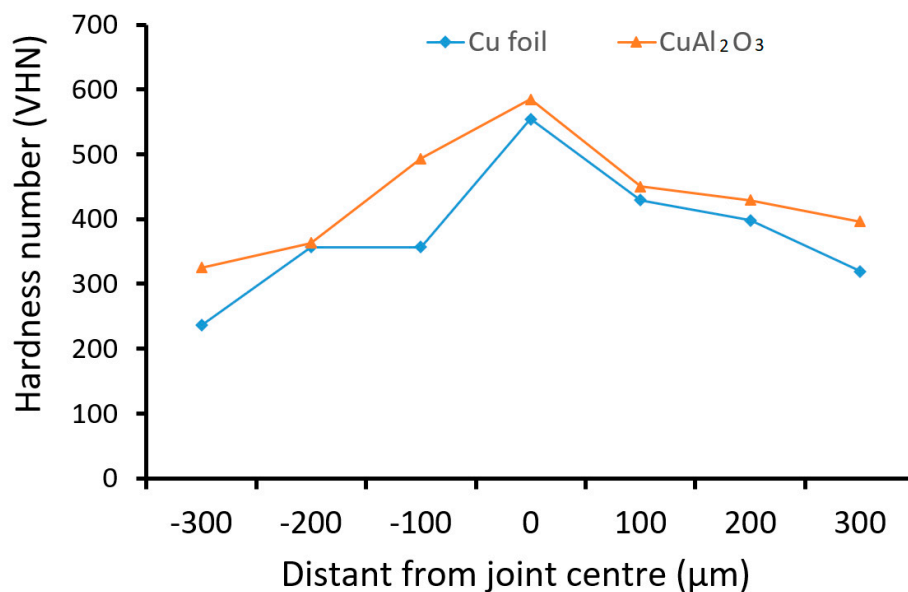


**Figure 13.** Hardness measurements as a function of interlayer composition for samples bonded at 850 °C for 30 min.

*3.5. Growth Kinetics of Interfacial Phases*

The width of the reaction layer was measured as a function of bonding time and bonding temperature and plotted as shown in Figure 14. The data indicate that as the bonding time increased, the width of the reaction layer also increased as predicted by the power law shown in Equation (1). Similar behavior was observed when the bonding temperature was increased from 800 to 900 °C. This response is believed to be consistent with the changes in the rate constant as the bonding temperature

increased. The width of the reaction layer increased with increasing bonding temperature and can be estimated by the mathematical relationship shown in Equation (1):

$$d = kt^n \tag{1}$$

where $d$ is the thickness of the reaction layer, $k$ is the rate factor, $t$ the diffusion time, and $n$ the time exponent. Further, $k = k_o e^{-\left(\frac{Q}{RT}\right)}$, where T is the bonding temperature (K), Q is activation energy (kJ/mol), R is the real gas constant (8.314 J/K mol), and $k_o$ is the growth constant (m$^2$/s). The growth kinetics of the intermetallic layer is controlled by interdiffusion (volume diffusion); therefore, the diffusion time is estimated to be $t^{1/2}$ (i.e., $n = 0.5$). On the other hand, if the growth kinetics was controlled by interfacial diffusion, the time exponent would be $n = 1$ [21,22].
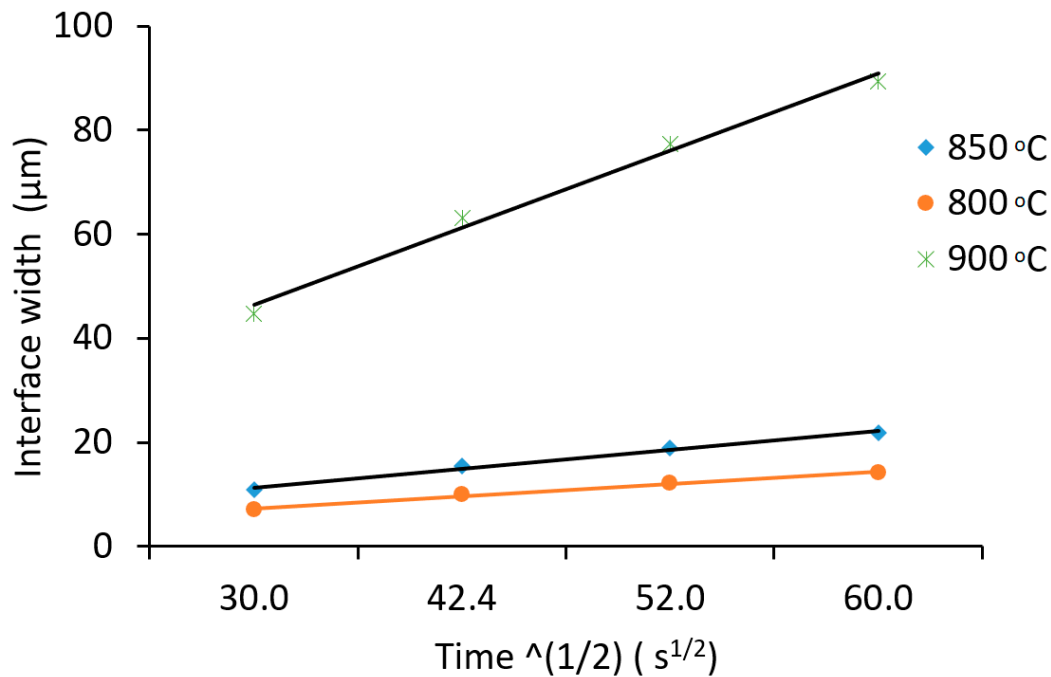


**Figure 14.** Variation of the width of the reaction layer as a function of the diffusion bonding conditions.

The results of the experimental study were used to assess the kinetics leading to the formation of the Ti$_2$Cu reaction layer at the interface. A summary of the growth kinetics of the reaction layer is shown in Table 3. The activation energy was calculated to be 111.4 kJ/mol for a bonding temperature of 850 °C. This is similar to findings published in the scientific literature which suggest that the activation energy for the formation of Ti$_2$Cu is approximately 122.1 kJ/mol [16]. In this study, the calculation of the activation energy was performed based on a simplified diffusion model, which assumes diffusion in a single phase which is influenced by the thickness of the reaction layer formed during the diffusion bonding process and the increases in the rate coefficient. The width of the diffusion layer is also believed to be driven by the diffusion of Cu into the Ti base metal, leading to the formation of various compounds. The Thermo-Cal model predicted the possible formation of several other compounds at the interface; however, the limitation of the simplified diffusion model is that only a single phase is assumed to have formed at the interface.

**Table 3.** Growth kinetics of the reaction $Cu_2Ti$ layer during the diffusion bonding process.

| Bonding Temperature (K) | Interlayer Thickness (µm) | Rate Coefficient k (µm/s$^{1/2}$) | Q (kJ/mol) |
|---|---|---|---|
| 1073 | 10 | 0.236 | 110.3 |
| 1123 | 15.4 | 0.362 | 111.4 |
| 1173 | 63.2 | 1.482 | 102.6 |

### 3.6. Mechanism of Bond Formation

The diffusion bonding process involves several stages [13]. The first stage involves initial contact between the faying surfaces and the interlayer, followed by deformation of the surface asperities under the effects of an externally applied load. The combination of heat and load increases the area of contact between the base metals and the interlayer and closes some of the voids or cavities present at the interlayer/base metal interfaces.

The second stage of bonding occurs due to interdiffusion between the base metals and the interlayer, leading to the formation of an intermetallic compound at the interface, which promotes the closing of remaining voids and cavities. The third stage of bonding involves diffusion of Cu into the SDSS and Ti–6Al–4V base metals, leading to a eutectoid reaction as predicted by the equation $\beta - Ti = \alpha - Ti + Ti_2Cu$ for bonding temperatures of 850 °C and below. The EDS analysis presented in Table 2 shows that intermetallic compounds such as $CuTi_2$ and $Cu_2Ti$ are also formed at the interface during the bonding process. A schematic of the mechanism involved in the bond formation is shown in Figure 15. The results show that the width of the reaction layer increases with increasing bonding time. Similarly, the literature shows that the strength of the bond increases with increasing thickness of the reaction layer. When a bonding temperature of 900 °C is used, a eutectic liquid forms at the interface, as illustrated in Figure 15E, and solidifies isothermally in the subsequent stages of the bonding process. At temperatures below 900 °C, solid-state bonding is achieved.
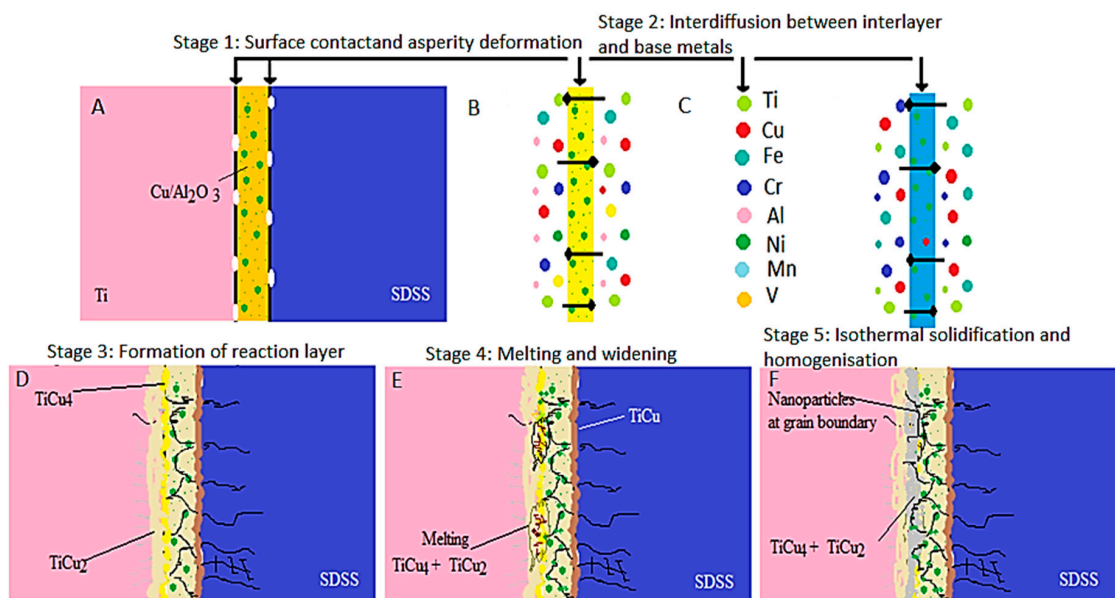


**Figure 15.** A schematic of the mechanism involved in bond formation of Ti–6Al–4V and super-duplex stainless steel using a $Cu/Al_2O_3$ interlayer: (**A**) Initial surface contact and asperity deformation; (**B,C**) Interdiffusion between interlayers and base metals; (**D**) Formation of the reaction layers; (**E**) Eutectic melting which occurs in samples bonded at 900 °C; (**F**) Isothermal solidification and homogenization of the interface.

## 4. Conclusions

In this study, Ti–6Al–4V alloy was diffusion bonded to super-duplex stainless steel (SDSS) using an electrodeposited Cu interlayer containing alumina nanoparticles to determine the effects of bonding parameters on the microstructural evolution within the joint region.

- The results of the study showed that SDSS and Ti–6Al–4V can be successfully diffusion bonded using a Cu interlayer embedded with alumina nanoparticles at temperatures above 800 °C.
- The combination of longer bonding time and high bonding temperature leads to the formation of various Ti–Cu intermetallic compounds within the interface. The use of a Cu interlayer prevented the formation of the more brittle intermetallic compounds of Fe–Ti and Ti–C.
- The addition of $Al_2O_3$ nanoparticles was successful in restricting the growth of a continuous intermetallic layer and caused a change in the volume, size, and shape of the intermetallic compounds formed by pinning grain boundaries and restricting grain growth.

**Author Contributions:** Formal analysis, K.O.C. and M.A.S.; Funding acquisition, T.I.K.; Investigation, K.O.C., and A.R., and M.A.S.; Methodology, M.A.S.; Project administration, T.I.K.; Resources, T.I.K.; Supervision, T.I.K.; Writing—original draft, K.O.C.; Writing—review and editing, K.O.C. All authors have read and agreed to the published version of the manuscript.

## References

1.  Muhamed, M.; Omar, M.; Abdullah, S.; Sajuri, Z.; Zamri, W.W.; Abdullah, M. Brazed Joint Interface Bonding Strength of AR500 Steel and AA7075 Aluminium Alloy. *Metals* **2018**, *8*, 668. [CrossRef]
2.  Suoranta, R.; Kah, P.; Martikainen, J.; Magnus, C. Techniques for joining dissimilar materials: Metals and polymers. *Rev. Adv. Mater. Sci.* **2014**, *36*, 152–164.
3.  Pardal, G.; Ganguly, S.; Williams, S.; Vaja, J. Dissimilar metal joining of stainless steel and titanium using copper as a transition metal. *Int. J. Adv. Manuf. Technol.* **2016**, *86*, 1139–1150. [CrossRef]
4.  Satoh, G.; Yao, Y.L.; Qiu, C. Strength, and microstructure of laser fusion-welded Ti-SS dissimilar material pair. *Int. J. Adv. Manuf. Technol.* **2013**, *66*, 469–479. [CrossRef]
5.  Kumar, N.N.; Ram, G.D.J.; Bhattacharya, S.S.; Dey, H.C.; Albert, S.K. Spark Plasma Welding of Austenitic Stainless Steel AISI 304L to Commercially Pure Titanium. *Trans. Indian Inst. Met.* **2015**, *62*, 289–297. [CrossRef]
6.  Shakil, M.; Tariq, N.H.; Ahmad, M.; Choudhary, M.A.; Akhter, J.I.; Babu, S.S. Effect of ultrasonic welding parameters on microstructure and mechanical properties of dissimilar joints. *Mater. Des.* **2014**, *55*, 263–273. [CrossRef]
7.  Verma, J.; Taiwade, R.V. Effect of welding processes and conditions on the microstructure, mechanical properties and corrosion resistance of duplex stainless steel weldments—A review. *J. Manuf. Process.* **2017**, *25*, 134–152. [CrossRef]
8.  Buffa, G.; Fratini, L.; Micari, F. Mechanical and microstructural properties prediction by artificial neural networks in FSW processes of dual phase titanium alloys. *J. Manuf. Process.* **2012**, *14*, 289–296. [CrossRef]
9.  Tanaka, K.; Nakazawa, T.; Sakairi, K.; Sato, Y.; Kokawa, H.; Omori, T.; Ishida, K. Feasibility of Iridium Containing Nickel Based Superalloy Tool to Friction Stir Spot Welding of High Strength Steel. *Miner. Met. Mater. Ser.* **2017**, 29–35. [CrossRef]
10. Bakavos, D.; Prangnell, P.B. Mechanisms of joint and microstructure formation in high power ultrasonic spot welding 6111 aluminium automotive sheet. *Mater. Sci. Eng. A* **2010**, *527*, 6320–6334. [CrossRef]
11. Akhtar, T.S.; Cooke, K.O.; Khan, T.I.; Shar, M.A. Nanoparticle enhanced eutectic reaction during diffusion brazing of aluminium to magnesium. *Nanomaterials* **2019**, *9*, 370. [CrossRef] [PubMed]
12. Atieh, A.M.; Khan, T.I. Application of Ni and Cu nanoparticles in transient liquid phase (TLP) bonding of Ti-6Al-4V and Mg-AZ31 alloys. *J. Mater. Sci.* **2014**, *49*, 7648–7658. [CrossRef]
13. Cooke, K.O.; Khan, T.I.; Oliver, G.D. Transient liquid phase diffusion bonding Al-6061 using nano-dispersed Ni coatings. *Mater. Des.* **2012**, *33*, 469–475. [CrossRef]

14. Cooke, K.O. A study of the effect of nanosized particles on transient liquid phase diffusion bonding Al6061 metal-matrix composite (MMC) using Ni/Al$_2$O$_3$ Nanocomposite Interlayer. *Metall. Mater. Trans. B* **2012**, *43*, 627–634. [CrossRef]

15. Balasubramanian, M. Characterization of diffusion-bonded titanium alloy and 304 stainless steel with Ag as an interlayer. *Int. J. Adv. Manuf. Technol.* **2016**, *82*, 153–162. [CrossRef]

16. Mo, D.F.; Song, T.F.; Fang, Y.J.; Jiang, X.S.; Luo, C.Q.; Simpson, M.D.; Luo, Z.P. A review on diffusion bonding between titanium alloys and stainless steels. *Adv. Mater. Sci. Eng.* **2018**, *2018*, 8701890. [CrossRef]

17. Taguchi, O.; Iijima, Y. Diffusion of copper, silver, and gold in α-titanium. *Philos. Mag. A Phys. Condens. Matter, Struct. Defects Mech. Prop.* **1995**, *72*, 1649–1655. [CrossRef]

18. van Beek, J.A.; Kodentsov, A.A.; van Loo, F.J.J. Phase equilibria in the CuFeTi system at 1123 K. *J. Alloys Compd.* **1995**, *27*, 97–103. [CrossRef]

19. Arzt, E.; Göhring, E. A model for dispersion strengthening of ordered intermetallics at high temperatures. *Acta Mater.* **1998**, *46*, 6575–6584. [CrossRef]

20. AlHazaa, T.I.K.A.; Haq, I. Transient liquid phase (TLP) bonding of Al7075 toTi–6Al–4V alloy. *Mater. Charact.* **2010**, *61*, 312–317. [CrossRef]

21. Furuto, A.; Kajihara, M. Numerical Analysis for Kinetics of Reactive Diffusion Controlled by Boundaryand Volume Diffusion in a Hypothetical Binary System. *Mater. Trans.* **2008**, *49*, 294–303.

22. Minho, O.; Kajihara, M. Kinetics of Solid-State Reactive Diffusion between Au and Al. *Mater. Trans.* **2011**, *52*, 677–684.